The front on the Northern Flank of Georges Bank in spring: 1. Tidal and subtidal variability

Andrew C. Dale,[1] David S. Ullman,[2] John A. Barth,[1] and Dave Hebert[2]

Received 29 January 2002; accepted 24 April 2003; published 3 September 2003.

[1] During March–April 1999, 2 weeks of undulating CTD and shipboard acoustic Doppler current profiler surveys revealed the variability of the intense internal tide on the northern edge of Georges Bank. The nature of the internal tide was modulated by episodic surface intrusions of cool, fresh Scotian Shelf Water (SSW), stratifying the otherwise vertically well-mixed outer bank. The introduction of SSW created a system analogous to that in summer, when the outer bank is thermally stratified and separated from well-mixed regions by a tidal mixing front. During SSW intrusions, internal tidal behavior is characterized by tidal advection that is significantly faster than internal wave propagation speeds on the bank (supercritical flow) and slower than the lowest internal modes in deeper water to the north (subcritical flow). A large-amplitude internal lee wave develops over the slope during off-bank tidal flow. This stalled energy is released to propagate on-bank as a high-frequency internal wave when the tide reverses. It is suggested, by analogy with the summer case, that a portion of this energy is used by mixing at the on-bank limit of SSW. The presence of SSW thus modifies the internal tidal response, enabling a mechanism that contributes to its assimilation with ambient bank water. The off-bank-propagating internal tide is dominated by a mode 1 internal wave at the M2 frequency, with cross-bank velocities comparable to the barotropic tide. *INDEX TERMS:* 4544 Oceanography: Physical: Internal and inertial waves; 4528 Oceanography: Physical: Fronts and jets; 4219 Oceanography: General: Continental shelf processes; *KEYWORDS:* Georges Bank, tidal mixing front, GLOBEC, internal tide, internal waves

Citation: Dale, A. C., D. S. Ullman, J. A. Barth, and D. Hebert, The front on the Northern Flank of Georges Bank in spring: 1. Tidal and subtidal variability, *J. Geophys. Res.*, *108*(C11), 8009, doi:10.1029/2002JC001327, 2003.

1. Introduction

[2] The Northeast Peak of Georges Bank and the adjoining slope to the Gulf of Maine (Figure 1) form a region where strong tides, steep topography and a background jet interact in a complex, nonlinear system. Associated with the bank edge is a broad frontal zone in which the transition of stratification and water properties from the bank to the gulf is governed by variation in tidal mixing and bank-edge processes. The nature of this frontal zone, and the exchanges that take place across it, are of considerable interest for their contribution to the fluxes of nutrients and zooplankton to and from the Georges Bank ecosystem.

[3] Georges Bank has been an intensively studied region, through a combination of observational programs and theoretical and modeling studies. The physical oceanographic setting, with emphasis on the Northern Flank and Northeast Peak, is summarized below. The current article describes hydrographic observations, obtained using a towed, undulating SeaSoar CTD, and concurrent shipboard Acoustic Doppler Current Profiler (ADCP) velocities in spring 1999 (March 30 to April 11). The survey region (Figure 1) extended from the Northeast Peak across the adjoining slope to the north into the eastern Gulf of Maine near its opening to the Northeast Channel. Winds during the period were variable, to 15–20 m s^{-1}, with a bias toward northerly (Figure 2). The data set has similarities with a 2-day data set from July 1988 [*Loder et al.*, 1992] which led to a greater appreciation and understanding of the nonlinear internal tidal phenomena of the bank edge. The system in spring differs from that in summer in that the outer edge of the bank is typically well-mixed vertically and has not yet become thermally stratified. Exceptions occur during intermittent periods when stratification is supplied by cool, fresh surface water of Scotian Shelf origin crossing the edge of the bank. These "cross-over" events have potentially important consequences for the supply of biota to Georges Bank [*Hannah et al.*, 1997].

[4] The spring 1999 data set will be presented in two parts. Part one (this paper) provides a description of the observed hydrographic structure, principally the tidal and internal tidal features and their low frequency (subtidal) variability. A companion article, part two [*Ullman et al.*,

[1]College of Oceanic and Atmospheric Sciences, Oregon State University, Corvallis, Oregon, USA.
[2]Graduate School of Oceanography, University of Rhode Island, Narragansett, Rhode Island, USA.

0148-0227/03/2002JC001327$09.00

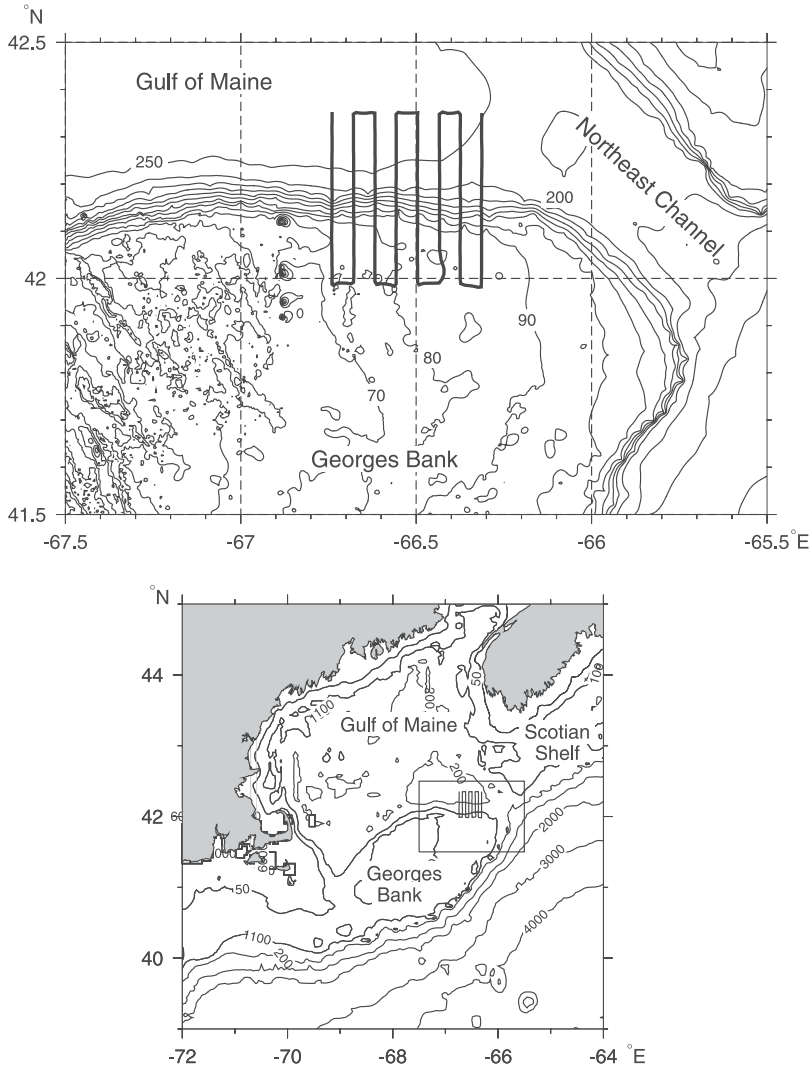

Figure 1. Survey region on the Northern Flank of Georges Bank. Typical ''radiator pattern'' and ''butterfly'' surveys are superimposed. Depths are in meters.

2003] investigates small-scale structure, mixing and cross-frontal fluxes.

2. Physical Background

[5] The topography of the Northeast Peak of Georges Bank shoals gradually to the west, from 100 m to less than 50 m (Figure 1), with the bank edge to the north aligned east-west and marked by a sudden change of gradient as the bottom drops to over 250 m in the Gulf of Maine. Maximum bottom slopes approach 0.025 (Figure 3). Hydrography [*Flagg*, 1987] shows a seasonal pattern controlled by the cycle of solar heating and wind-induced mixing. In the Gulf of Maine, relatively warm, saline Maine Bottom Water (MBW) occupies the lower part of the water column, with isopycnals bending downward to intersect the northern slope of Georges Bank. The shallower summer water masses, Maine Intermediate Water (MIW) and warm, fresh Maine Surface Water (MSW), become largely homogenized in winter, although relatively cool, fresh Scotian Shelf Water (SSW) may override them in the east. This SSW travels south along the Scotian Shelf, but typically ''turns the corner'' to make a circuit around the Gulf of Maine before reaching Georges Bank as a late-summer salinity minimum [*Bisagni and Smith*, 1998]. At times, however, it breaks free of topographic constraints and crosses the Northeast Channel onto the eastern or southern parts of Georges Bank, bringing low salinities in spring. This process occurs with pronounced interannual variability [*Bisagni et al.*, 1996], and mechanisms are poorly understood, although eddy activity in the Northeast Channel may be important [*Bisagni and Smith*, 1998].

[6] Shallow areas of Georges Bank are well-mixed vertically by tidal stirring throughout the year, although the composition of the well-mixed water over the bank varies interannually [*Houghton and Fairbanks*, 2001]. Seasonal heating stratifies deeper regions of the bank in summer, with a tidal mixing front typically located around the 60-m isobath from May to September/October [*Mavor and Bisagni*, 2001]. The location of this front is controlled by the balance between buoyancy input through heating and tidal stirring related to bottom depth and tidal velocity

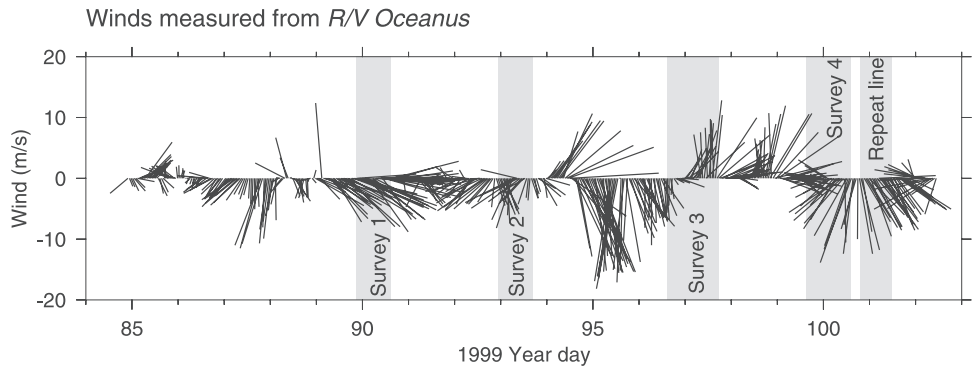

Figure 2. Winds measured from R/V *Oceanus* during the survey period. Sticks point downwind.

[*Simpson and Hunter*, 1974]. In winter, the boundary between the tidally mixed regime and the Gulf of Maine water masses tends to coincide with the bank edge, but has little surface expression. Climatological analysis of sea-surface temperature fronts [*Mavor and Bisagni*, 2001] reveals that during January–April, temperature fronts marking the edge of SSW may occur over a broad region extending from the summer location of the tidal mixing front on the bank out into the eastern Gulf of Maine and the Northeast Channel.

[7] Tidal currents over Georges Bank are dominated by the M2 constituent which, on the Northeast Peak, is larger than the two next largest constituents, N2 and S2, by 4.2 and 4.8 times, respectively [*Brown and Moody*, 1987]. M2 currents exceed 1 m s^{-1} in the shallowest regions, for a tidal excursion approaching 15 km, with a decrease in amplitude and advance in phase near the bottom due to frictional effects. M2 current ellipses are oriented such that their principal axis is almost normal to the bank edge. This combination of a strong cross-topography component of the barotropic tide and relatively abrupt bottom slope creates conditions favorable to the generation of an energetic internal tide. Previous descriptions of the internal tide in the region have been based on mooring time series [*Magnell et al.*, 1980; *Marsden*, 1986], rapid cross-bank sections using a towed profiler [*Loder et al.*, 1992; *Brickman and Loder*, 1993; *Loder et al.*, 1993] and modeling studies [*Lamb*, 1994; *Chen and Beardsley*, 1998]. The system is characterized by barotropic tidal advection over the bank that at most times is faster than internal wave propagation speeds, leading to complex, nonlinear behavior at the bank edge. With summer (thermal) stratification of the bank, peak off-bank tidal flow has a Froude number, relative to a mode 1 internal wave, of around 3 on the bank and 0.3 in deeper water [*Loder et al.*, 1992]. Internal wave energy concentrates near the bank edge as a steep depression of the density structure and possible hydraulic jump. As the tide reverses this energy is released, apparently propagating on-bank as a pair of internal wave packets which potentially supply a significant contribution to the energy budget of the tidal mixing front [*Brickman and Loder*, 1993]. Mooring data [*Marsden*, 1986] have revealed that M2 velocities in deep water north of Georges Bank have pronounced vertical structure reflecting an off-bank-propagating (linear) internal tidal component of comparable amplitude to the barotropic tide. Sun-glitter images also suggest nonlinear internal wave packets propagating off-bank to the north [*La Violette et al.*, 1990].

[8] Eulerian current measurements [*Butman et al.*, 1982, 1987] reveal an eastward jet over the Northern Flank of Georges Bank, part of a general clockwise circulation around the bank. Mean Eulerian velocities are around 0.3 m s^{-1} with evidence for a seasonal cycle [e.g., *Naimie*, 1996]. Flow is weakest in late winter/early spring and strongest in late summer/early fall. The jet appears to be driven by a combination of baroclinic pressure gradients and topographic rectification of tidal currents over the slope [*Loder*, 1980], with both mechanisms important in summer [*Loder and Wright*, 1985]. The ellipticity of tidal orbits combined with horizontal and vertical gradients of tidal amplitude lead to Stokes' drift, which adds a Lagrangian flow component, opposing the mean Eulerian flow.

3. Methods

3.1. SeaSoar and ADCP Data Collection

[9] Data described here were obtained using a SeaSoar undulating CTD and shipboard ADCP. The SeaSoar was instrumented with dual pumped conductivity and temperature sensors as well as a pressure sensor, fluorometer, and

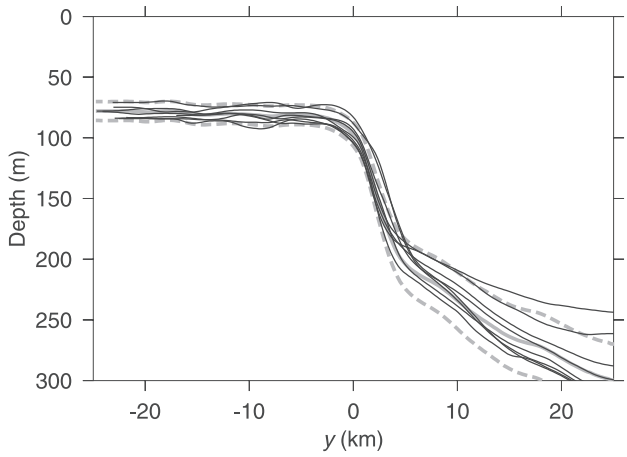

Figure 3. Bottom depth $h(y)$ on the principal north-south survey lines, compared to a mean section $\bar{h}(y)$ (shaded line). Dashed shaded lines show the mean ±10%. Sections have been aligned on the bank edge ($y = 0$), defined as the point where $h_y = 0.01$.

transmissometer. This configuration of sensors and the subsequent processing of SeaSoar data have been described in detail by *Barth et al.* [2000].

[10] Temporal and spatial variability were investigated through a series of 35 north-south sections, normal to the bank edge, each of around 40 km in length and 3 hours duration (at a survey speed of 7 knots). Four "radiator pattern" surveys (Figure 1) comprised 7, 7, 8, and 8 such sections, respectively, having an east-west separation of 5 km. In addition, a sequence of five repeats were made of a single north-south line. Sections will be referred to by their survey number (1–4), or R for the repeated line, and a letter code (a–h) giving a temporal order within each survey. So, for instance, the second north-south section of survey 3 is denoted 3b. The sequence of lines was east-west in surveys 1, 2, and 3, and west-east in survey 4. Lines bracketed the bank edge in the longitude range 66.75°W to 66.3°W. Because the time to make each section was roughly one quarter of a semidiurnal tidal period, they are not instantaneous with respect to tidal phase, and the direction of phase advance depends on ship direction.

[11] During the time between radiator surveys, isopycnal floats were released and tracked as the SeaSoar was towed in a "butterfly" pattern around the float location (Figure 1). This provided much additional data in a region extending for 20 km to the north of the bank edge.

[12] When towed at 7 knots and cycling between near the surface and 110 m (a typical depth attained in deep water) the wavelength of SeaSoar undulations was approximately 1 km. Over Georges Bank, cycling to only 60 m depth, wavelength was closer to 300 m. At a given depth level, an undulating instrument makes an observation twice per cycle, once on the upcast and once on the downcast. The horizontal spacing of data points in the central water column is thus roughly half the undulation wavelength. The spatial resolution of a survey is anisotropic, differing between the east-west direction (line spacing, 5 km) and the north-south direction (half the undulation wavelength, 0.15–0.5 km, depending on depth). Advection during an ongoing survey means that the effective physical separation of observations is not necessarily the same as the apparent spacing of the survey locations (see next section).

3.2. Advection of the Survey Grid as an Aid to Interpretation of Horizontal Fields

[13] Interpretation of data from a survey grid in a highly dynamic environment requires care to separate true spatial structure from slow temporal evolution and aliased high-frequency variability. Here an attempt has been made to avoid such problems by advecting observations from each survey to a common time (the survey start time) using barotropic mean and tidal velocity fields. These fields have been estimated by a method similar to *Candela et al.* [1992] using ADCP velocities from this cruise (R/V *Oceanus*) and from a parallel cruise of R/V *Endeavor*. The analysis was for four tidal constituents (M2, S2, K1, and O1), with horizontal structure of the mean and tidal velocities represented by second-order and linear polynomial functions, respectively. The record length is not strictly long enough to separate nearby constituents; however, the purpose of this analysis was simply to provide as good a fit as possible to the velocity record during the cruise period. As such, both M2 and S2 are needed to represent the spring-neap cycle, and the analysis should not be judged on the criteria of more general tidal analyses. Advected observations provide a more synoptic view of the system, since the primary source of advective distortion, the barotropic tide, has been well represented. There is, however, clearly much structure to the velocity field that has not (and cannot be) represented. Vertical advection is difficult to estimate and so has been neglected, as have vertical structure of the mean and tidal velocity fields and time evolution due to non-advective processes.

3.3. Collapse of the Three-Dimensional Data Set to Two Dimensions

[14] For the purpose of determining the long-term mean and tidal structure, the full, three-dimensional data set will be collapsed into a single two-dimensional, vertical, cross-bank (north-south) section. For now, justification for this collapse of the along-bank (essentially east-west) dimension will be limited to the observation that the topography is highly two dimensional, albeit with a gradual shallowing of the summit of the bank to the west, and that, as described above, the bank edge forms a frontal region where cross-bank gradients are much greater than along-bank. Additional, more quantitative, evidence that the collapse to two dimensions is justifiable will emerge from this data set, and a more extensive discussion of this aspect can be found in section 5. The motivation for this procedure is that the effective data coverage, both spatial and temporal, is greatly increased within the remaining two dimensions. Although the temporal resolution still does not approach that of mooring data, it will be seen that it is sufficient to calculate long-term mean velocity and hydrographic fields with some degree of confidence, as well as to perform a harmonic analysis for the M2 tide, revealing the spatial (cross-bank and vertical) tidal structure.

[15] In collapsing the data set onto a single cross-bank section, one problem to be resolved was how to overlay north-south sections at different longitudes and with slightly different topographies. The solution was to introduce a small vertical distortion. An observation at latitude, longitude, vertical position, and time $(\tilde{x}, \tilde{y}, \tilde{z}, \tilde{t})$ is transformed to coordinates (y, z, ϕ) where y is distance north of the bank edge, z is a stretched vertical coordinate, and ϕ is the M2 tidal phase relative to astronomical forcing at Greenwich. The bank edge is defined as the location where the northward depth gradient is 0.01, the latitude of which has been estimated for discrete values of $\tilde{x}$ corresponding to the principal north-south survey lines (Figure 3). The vertical coordinate z is obtained by converting to a Σ coordinate $\Sigma = \tilde{z}/h$ using the local bottom depth $h(\tilde{x}, \tilde{y})$ then rescaling by a mean depth profile $\bar{h}(y)$ to give $z = \Sigma\bar{h} = z\bar{h}/h$. The advantage of this procedure is that both the surface and bed of any observed section transform to the surface and bed of the "standard" section. Of course, this involves some inherent vertical distortion, because the topography varies gradually from east to west, even when aligned on the bank edge, but in practice $\bar{h}/h$ typically differs from unity by less than 10% (Figure 3).

[16] With all observations placed in the standard spatial and phase coordinates (y, z, ϕ) it is apparent that there are some biases in the data coverage (Figure 4). The survey was

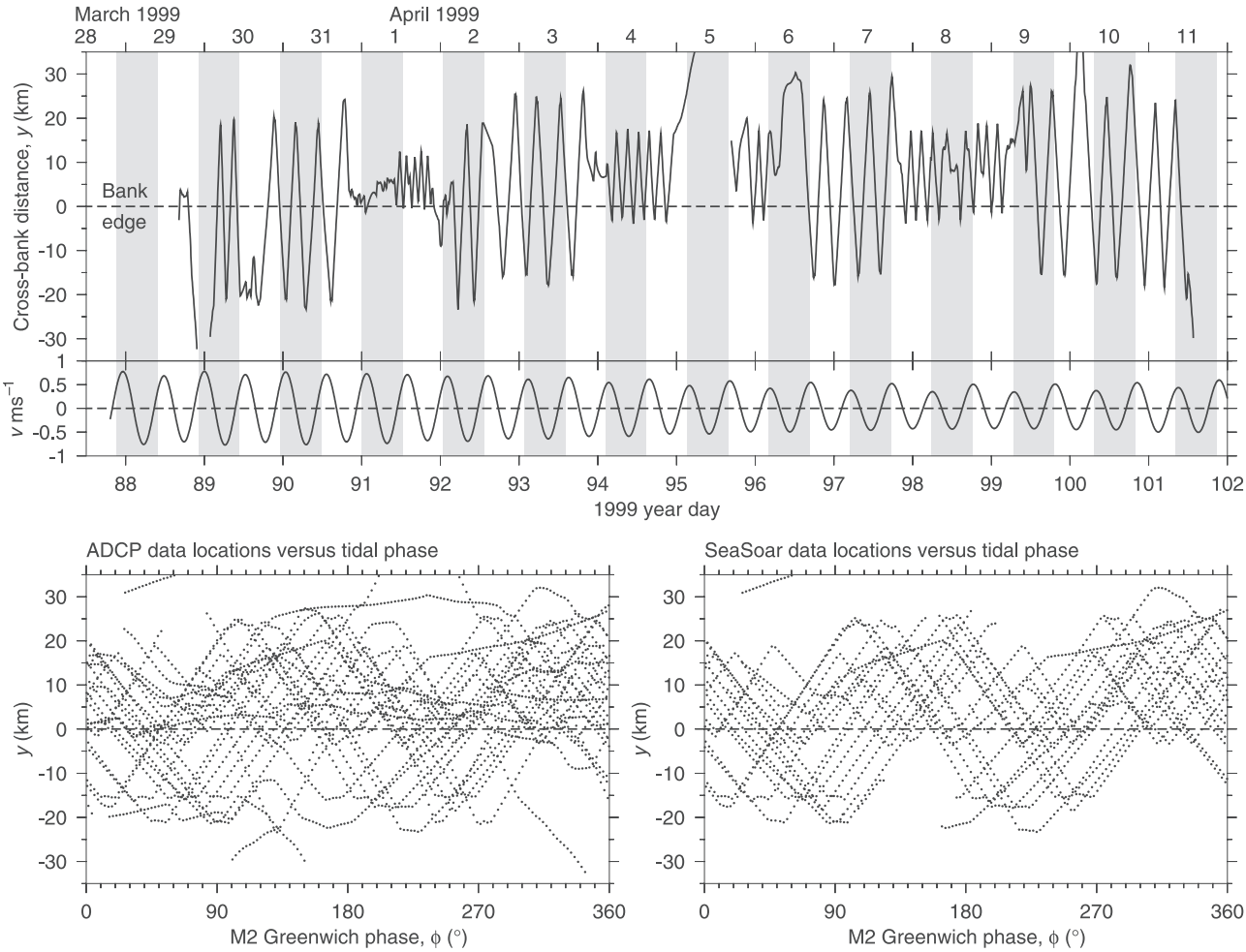

Figure 4. Time series of ship cross-bank position y (km) and predicted tidal velocities at 66°30′W, 42°05′N (on the bank and central to the survey region). Shaded bars show M2 tidal cycles. Bottom panels show the distribution of ADCP and SeaSoar data points versus cross-bank position (y) and M2 Greenwich phase (ϕ).

concentrated within 20 km of the bank edge, but favored deeper water, where tracking of the isopycnal floats was carried out. The long survey lines gave coverage equally weighted about the bank edge. Plotting data points in the space (ϕ, y) of position relative to the bank edge versus tidal phase reveals that in substantial phase ranges (e.g., near 135° and 315° phase) there is little SeaSoar data from over the bank ($y < 0$). ADCP data coverage has fewer such phase gaps because the ADCP was operational during periods when the SeaSoar was not deployed.

3.4. Long-Term Means

[17] The long-term mean cross-bank structures of velocity and hydrography in the standard two-dimensional coordinate system are calculated with care to avoid a bias with respect to tidal phase. Observations are first transformed to the standard coordinates (y, z, ϕ) then binned with intervals $\Delta z = 5$ m, $\Delta y = 1$ km. The tidal cycle is split into eight M2 phase intervals (1–8 in Figure 5), and mean sections are calculated in each phase interval by calculating the mean in each spatial bin. A final, phase-averaged mean for each bin is the equally weighted mean of the eight phase intervals (Figure 5). Spatial bins for which one or more phase intervals have no data are discarded, although those bins on the bank with two missing phase bins separated by 180° (Figure 4) are retained. Resulting mean fields should be regarded as not just temporally averaged but also spatially averaged in the along-bank direction through the collapse of the data set to two dimensions. Subtidal variability in the data set includes three-dimensional perturbations of hydrographic fields due to the advection of anomalies, variation in mixed layer depth in response to changes in wind stress, and effects of changes in tidal mixing on the spring-neap cycle.

3.5. M2 and M4 Harmonic Analysis

[18] A harmonic analysis for the M2 tidal component is performed by determining the least squares best fit M2 period sine function to the "time series" of perturbations to the phase-averaged mean in each (Δy, Δz) bin (Figure 5). This procedure is more appropriate to perturbations of velocity than of scalar quantities (temperature, density, etc.). In the Georges Bank region, tidal excursions are comparable to the lengthscales of scalar fields, so scalar

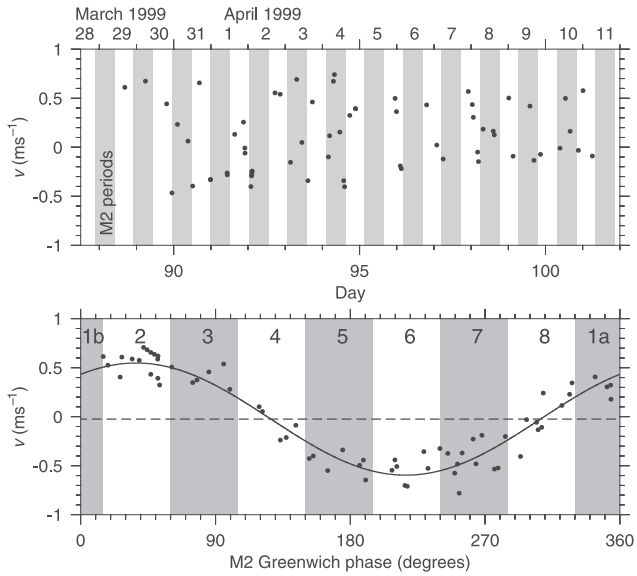

Figure 5. Time series of v in a bin centered at $y = 0$ km, $z = -30$ m, one of the more densely surveyed locations. In the top panel, shaded bars represent M2 tidal periods. During each tidal cycle, between zero and eight observations were made in this bin. In phase space (bottom panel), a phase-averaged mean velocity (dashed line) is computed by taking the mean in each of the labeled phase intervals 1 to 8, then taking the mean of these eight. The solid line is a best fit M2 period sine curve to the perturbations from this phase-averaged mean.

gradients, as viewed from a fixed location, vary over a tidal cycle. Even perfectly sinusoidal advective velocities would not produce a sinusoidal perturbation of the scalar.

[19] The result of the M2 harmonic analysis will, somewhat loosely, be referred to as the "linear" M2 tide, the component which remains at the forcing frequency, containing both barotropic and baroclinic components. Nonlinear features of the M2 tide are not represented. It is straightforward to extend the analysis to the M4 constituent, the first harmonic overtone of M2 with a period of half that of M2 (M4 = 6.21 hours, M2 = 12.42 hours). M4 reveals distortion of sinusoidal M2 perturbations, and may indicate nonlinearity.

3.6. Froude Number

[20] A cross-bank Froude number is calculated by solving the vertical structure eigenvalue problem for linear internal waves,

$$(\sigma^2 - f^2)\frac{\partial}{\partial z}\left(\frac{\partial p/}{N^2 - \sigma^2}\right) = -k^2 p, \qquad (1)$$

where $p(z)$ is a pressure perturbation, σ is frequency and k is wavenumber in the y direction. It is assumed that $f^2 \ll \sigma^2 \ll N^2$, the frequency range over which internal wave modes are nondispersive, so calculated phase speeds are applicable over a wide frequency range. This assumption is made by setting f to zero and making the hydrostatic approximation. Modal phase speeds at the M2 frequency, $\sigma_{M2} \approx 1.44f$, would be around 40% faster due to their proximity to f. The (generally small) vertical shear of the background velocity is neglected. Boundary conditions are $\partial p/\partial z = 0$ ($z = 0, -h$) representing a rigid lid and flat bottom. It should be noted that separation of vertical and horizontal structure and the consequent modal decomposition of the internal wave field is strictly valid only when the bottom is flat, an assumption which is justifiable over the summit of Georges Bank, and perhaps in the Gulf of Maine, but not over the slope.

[21] If the ith vertical mode $p_i(z)$ has phase speed $c_i = \sigma/k$, the Froude number of the cross-topography flow relative to this mode,

$$Fr_i = |\hat{v}/c_i|, \qquad (2)$$

is determined at points on the SeaSoar survey path, where $\hat{v}$ is the depth mean northward ADCP velocity and c_i is calculated for the observed density profile. In deep water, density is linearly extrapolated in z below the base of the SeaSoar data by assuming that it approaches a climatological value on the bottom.

4. Results

4.1. Three-Dimensionality and Temporal Variability of the Presence of Scotian Shelf Water (SSW)

[22] The primary source of three-dimensionality during the survey period was the variable presence of SSW at the surface. From the perspective of the survey grid, SSW was present over the bank during episodic "cross-over" events. These events produced significant along-bank gradients, which were otherwise small. Sea surface temperature (SST) images (Figure 6) reveal a cool patch off-bank to the northwest of the survey region, covering Browns Bank and the western part of the Northeast Channel. The shape of the patch shows evidence of mesoscale structure and significant evolution during the 8-day period between images. Because the survey region was located near the edge of this evolving patch, strong variability was observed.

[23] The advective procedure described in section 3.2 will be applied to two fields from the SeaSoar surveys: temperature at 5 m, and depth of the 32.5 psu isohaline. These fields are chosen to represent the distribution of SSW. Because SSW is relatively light, cool and fresh (Figure 7), it has an SST signature, although it is more clearly identified by its low salinity, especially over Georges Bank where temperature contrasts may be small. It is typical to regard a salinity of 32 psu as indicative of SSW [e.g., *Bisagni et al.*, 1996], so our choice of 32.5 psu represents a broader class of low-salinity surface water. It does, however exclude water from the vertically well-mixed regions of the bank which occurs within a relatively localized region of T-S space (Figure 7). At no time during the cruise did a vertically well-mixed water column have a salinity as low as 32.5 psu.

[24] A time series of advected fields from the four "radiator pattern" surveys (Figure 8) illustrates the temporal and spatial variability of SSW crossovers and frontal locations during a 10-day period. It is immediately apparent, from the distortion of the survey grid, that it is important to take advection into account when interpreting these surveys with time and length scales comparable to those of the tide. In addition, the eastward mean flow expands the effective spatial coverage of the east-west surveys (1, 2, and 4), while it compresses the single west-east survey (survey 3).

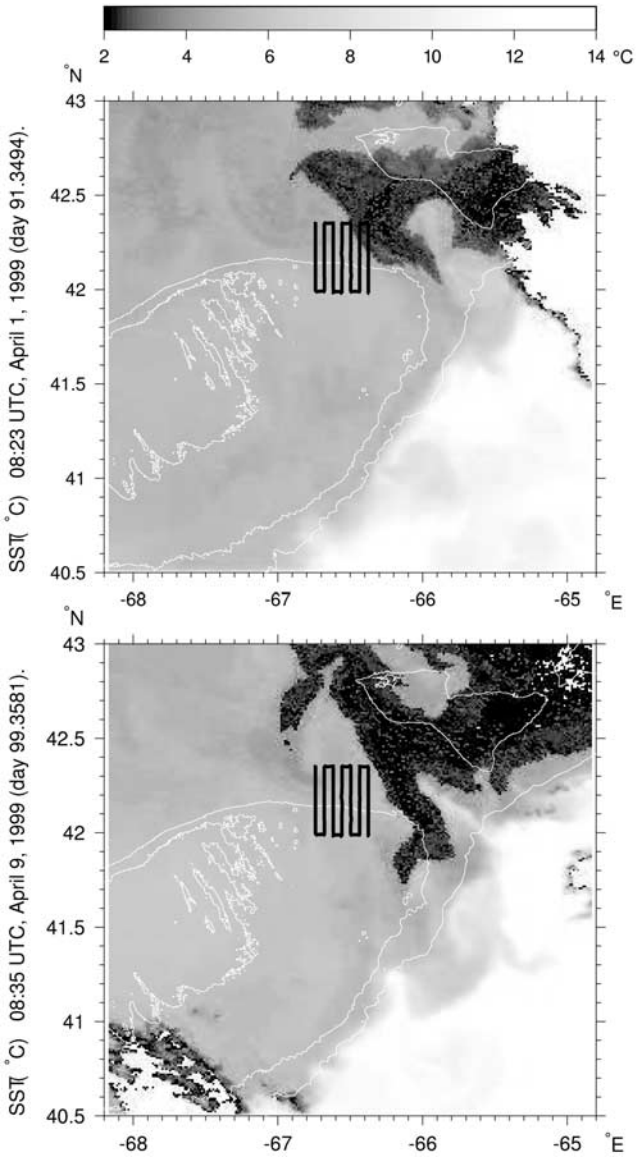

Figure 6. Sea surface temperature (SST) images from 0823 UTC, April 1, 1999 (day 91.3494) and 0840 UTC, April 9, 1999 (day 99.3581). Scotian Shelf Water (SSW) appears as dark (cool) to the northeast of the survey region. A typical survey grid is shown. Isobaths are at 50 m, 100 m, and 200 m. (Image was supplied by J. J. Bisagni.)

[25] Since the two advected fields are both indicators of SSW they show similar spatial patterns. At all times there was a tendency for a front to be located above, and slightly to the north of, the bank edge, around 42.2°N. Cool, fresh water over the bank occurred primarily in the east of the survey region, being most apparent during survey 3 and least apparent during survey 1, when it occurred only to the north of the bank edge. During survey 1, there is also an impression of lower than usual stratification in the bank edge/slope region (see raw sections, Figures 9 and 10) which may be because this survey coincided with spring tides (Figure 4), presumably a period of enhanced tidal mixing.

[26] Mean fields of temperature at 5 m and depth of the 32.5 psu isohaline have been calculated from the four advected survey fields (Figure 11). These means clearly show that north-south gradients dominate east-west gradients although there is a tendency toward cooler, fresher water in the east. The ratio of the mean $\partial/\partial y$ to $\partial/\partial x$ is 4.7 (temperature at 5 m) and 5.2 (depth of the 32.5 psu isohaline). Over the bank, south of 42.1°N, however, both gradients are relatively small and the alongbank gradient actually dominates.

4.2. Tidal Cycle When the Bank is Vertically Mixed

[27] SeaSoar sections have been partitioned into two groups based on whether the bank was vertically well-mixed or stratified (Figures 9 and 10). This partitioning was subjective, and sections showing patchy on-bank stratification were categorized as stratified. The mixed and stratified groups have each been ordered into a sequence based on M2 tidal phase, relative to astronomical forcing at Greenwich, at the time the survey ship passed over the bank edge ($y = 0$). The phase of maximum off-bank M2 flow at $y = 0$ is 30°–40° (varies with depth), although the phase of maximum flow of the total tide may lie outside this range due to the influence of other tidal constituents (see the velocity time series in Figure 4). As noted earlier, each section took around a quarter M2 period to complete, so phase varied significantly from start to finish and the ship direction should be taken into account (inset white arrow in the figures). The two ordered sequences are clearly not time series, nor do they represent sections at a single longitude.

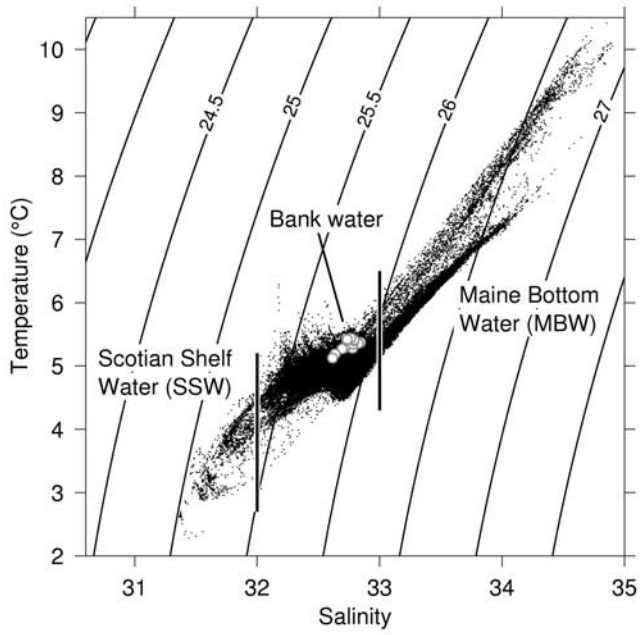

Figure 7. Temperature versus salinity for all water sampled by the SeaSoar (i.e., to depths of 110–120 m) within the ''radiator pattern'' survey region. Water encountered in the well-mixed regions of the summit of Georges Bank is identified by white disks. Contours are of σ_t. Scotian Shelf Water (SSW) is identified as all water with salinity less than 32 psu, and Maine Deep Water as water with salinity greater than 33 psu (both following *Flagg* [1987]).

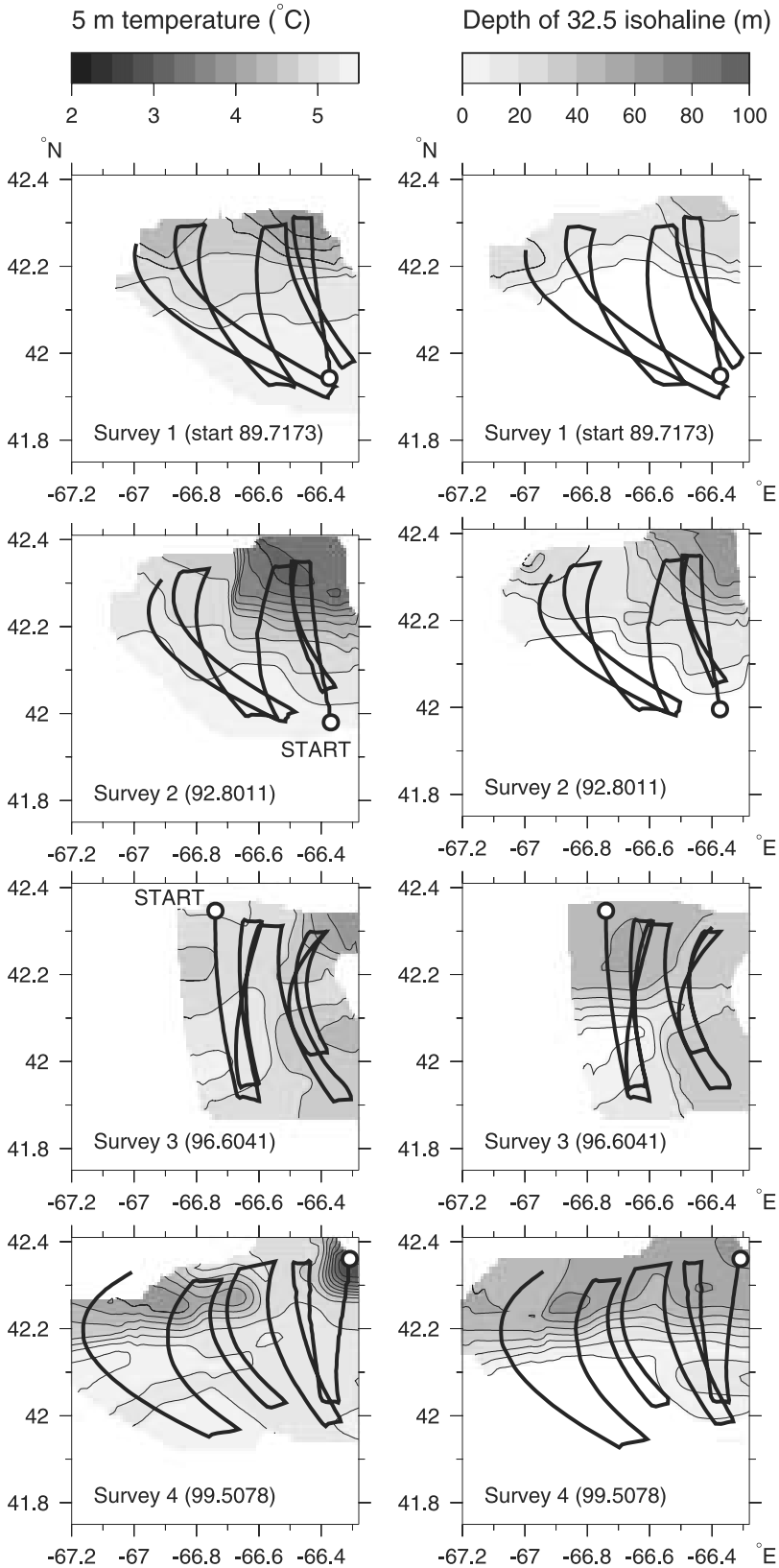

Figure 8. Fields of temperature at 5 m (left column) and depth (m) of the 32.5 psu isohaline (right column) on the four survey grids, advected to the start time of each survey (in brackets) using a polynomial horizontal fit to barotropic mean and tidal velocities. Advected survey grids are shown as bold lines, and the start of each survey is indicated by a white circle.

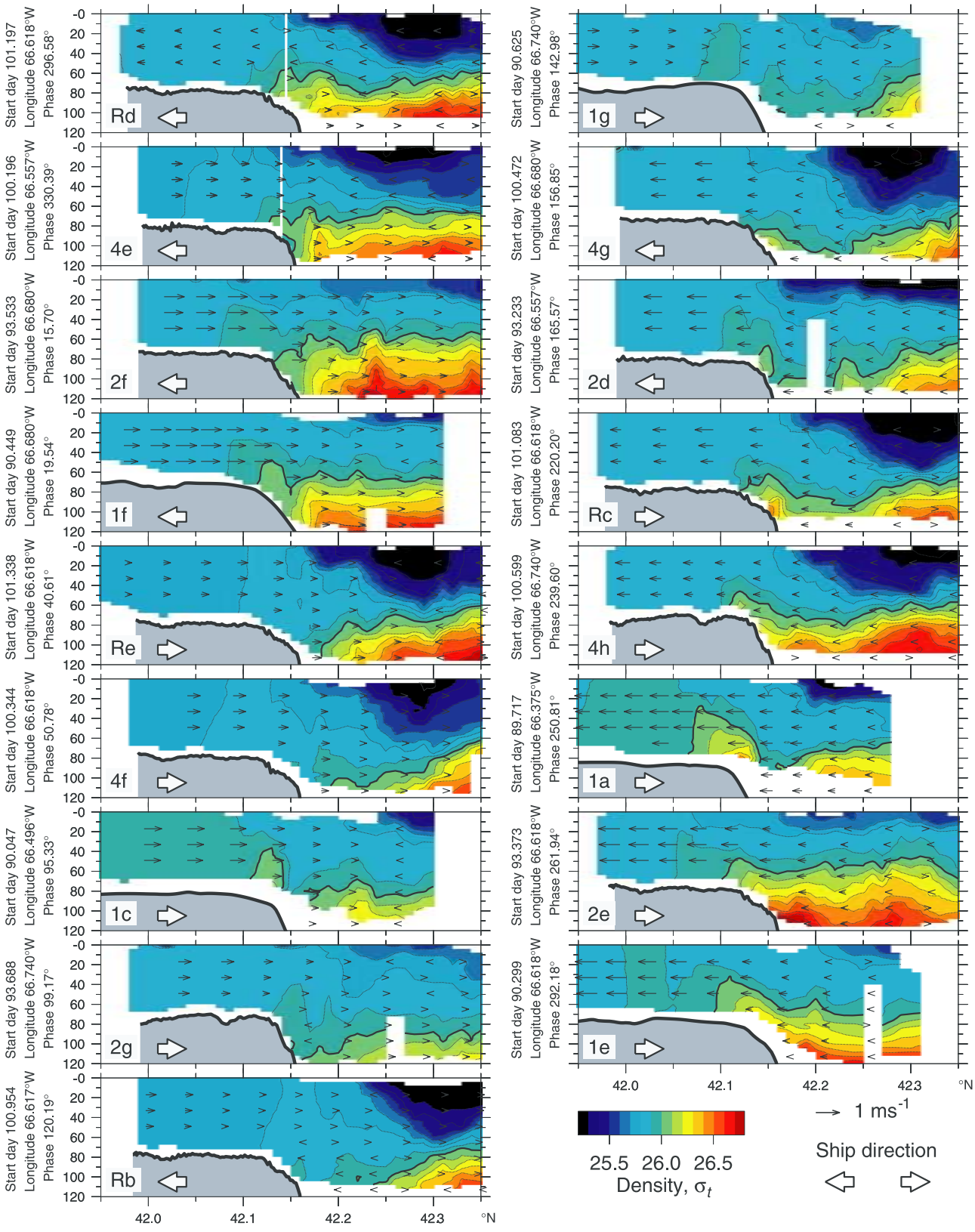

Figure 9. Cross-bank sections of density (σ_t) and north-south component of ADCP velocity (vectors), ordered by M2 phase at the time of crossing the bank edge (vertical white line). This sequence shows sections in which the bank was vertically well mixed. Survey of each section took a quarter tidal period, so phase variation and ship direction (inset white arrow) are significant. The start time (year day) and longitude of each section are given. Phase is relative to astronomical forcing at Greenwich. Labels refer to the survey (1–4, R) and temporal sequence within each survey (a–h).

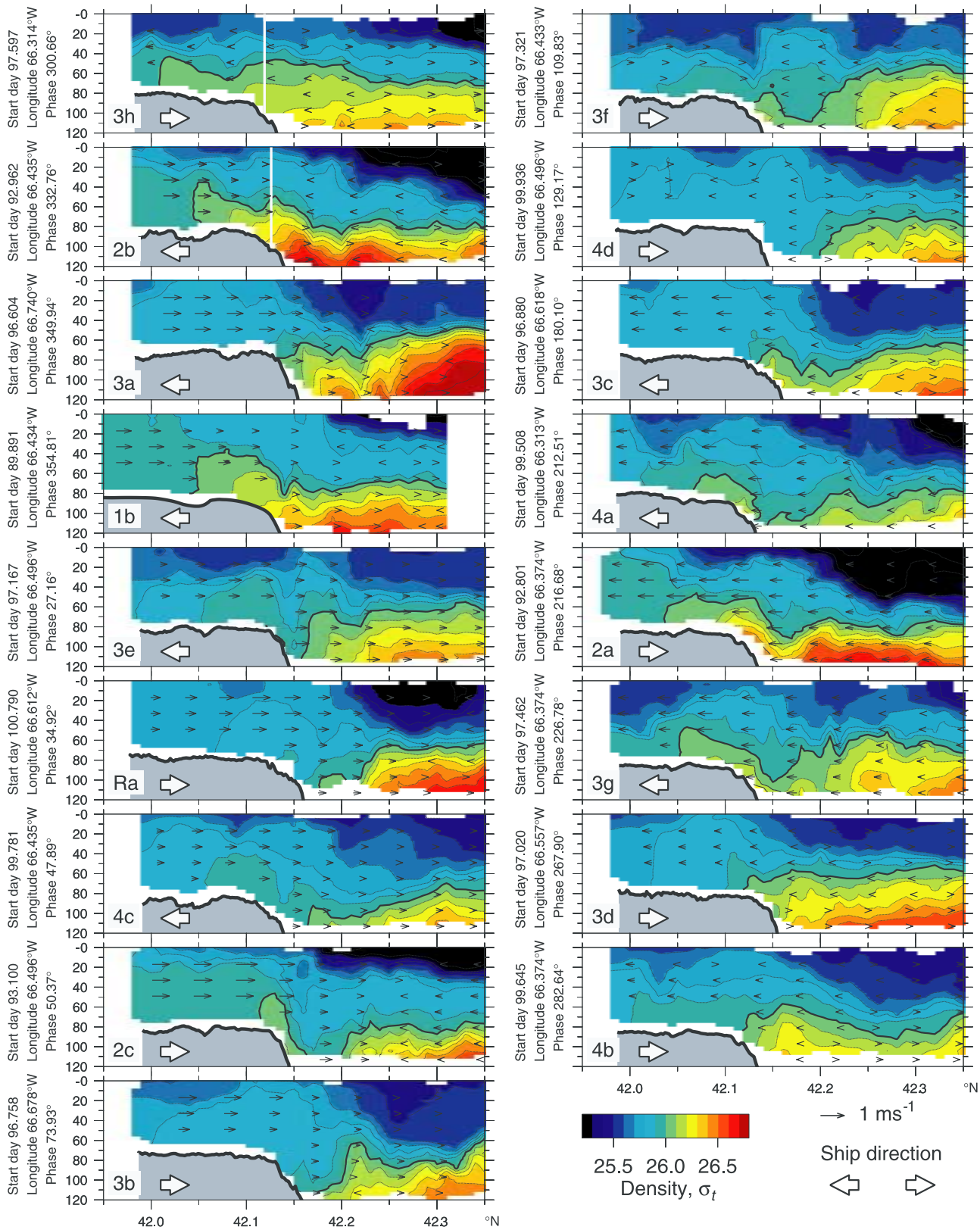

Figure 10. As in Figure 9 but at times when the bank was stratified.

They do, however, provide a summary of the features observed at varying tidal phases.

[28] When the bank was well mixed (Figure 9), off-bank stratification was advected back and forth across the bank edge during the tidal cycle. The steep topography ensured that isopycnals were distorted substantially during this process, primarily when relatively dense (warm, saline) Maine Bottom Water (MBW), identified by the bold

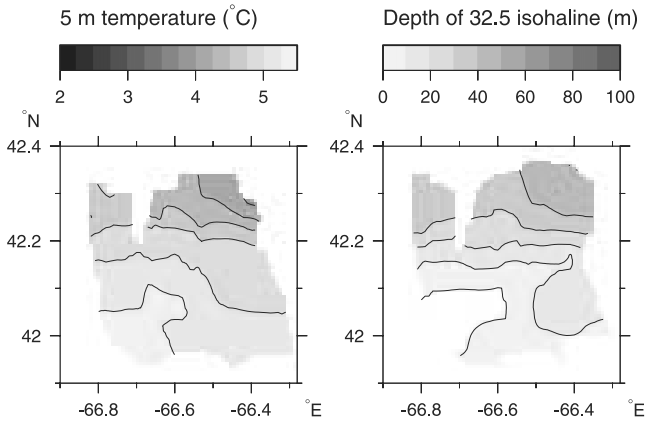

Figure 11. Mean fields of (left) temperature at 5 m and (right) depth (m) of the 32.5 psu isohaline, calculated over the four survey grids after advection to a common M2 phase. These fields are restricted to areas where the four advected surveys overlap.

$\sigma_t = 26$ kg m^{-3} contour (see Figure 7), was advected across the slope and pushed up as a tongue onto the outer bank. This on-bank MBW typically occupied the lower half of the water column and extended 5 km onto the bank at maximum extent. At times during the surveys, a vertically homogeneous column of relatively warm, saline water was present near the bank edge. It is cautiously suggested that these features represent mixing of MBW with existing bank water [*Ullman et al.*, 2003], although such a two-dimensional interpretation may be naive in the presence of strong advection along the bank edge. Examples can be seen in Figure 9 on lines 1e, 4f, and Rb. The column had a width of around 5 km and anomalies from surrounding bank water were small (0.05 kg m^{-3}, 0.1°C, 0.2 psu for lines Rb and Re). Reduced turbidity and chlorophyll fluorescence within the column (not shown here) were more typical of deeper water from the Gulf of Maine than of Georges Bank water.

[29] During times when the bank is well mixed, internal tidal energy generated by advection of stratified water across the bank edge must propagate northward, off-bank into the Gulf of Maine [e.g., *La Violette et al.*, 1990], since it cannot propagate onto the unstratified bank. On several lines, short, apparent high-frequency waves or wave packets were encountered (42.2–42.25°N on line 2f, 42.3–42.35°N on line 4g), although these were poorly resolved and there was no clear pattern to their occurrence.

4.3. Tidal Cycle When the Bank is Stratified

[30] When the bank is stratified by SSW, the system is analogous to the thermally stratified summer case [*Loder et al.*, 1992; *Brickman and Loder*, 1993]. Continuity of off-bank tidal flow over the steep bank edge requires a decrease in velocity. The resulting convergence and vertical motion displaces the density structure downward and stretches it vertically, distorting isopycnals to reflect the shape of the topography. North of the slope, where water columns do not encounter steep topography during a tidal cycle, this distortion does not occur, so the depression of the density structure develops into a localized, large-amplitude feature. The early stages of this process can be seen in survey section 1b of Figure 10, and fully developed depressions of over 50 m vertical amplitude were encountered on lines 3e and 2c. Internal wave energy tends to be retained over the slope as a lee wave because flow here is near-critical to low mode internal waves (discussed in the next section).

[31] When the tide reverses and begins to flow on-bank, stalled internal wave energy near the bank edge is able to propagate onto the bank. The sequence of survey sections 3e–3g illustrate the generation and release of one particular large amplitude internal wave. In survey section 3e, off-bank tidal flow was approaching its maximum at the bank edge. Isopycnals plunged downward over the slope, mirroring the topography and rebounding immediately downstream in a possible hydraulic jump. Vertical displacement of the 25.9 isopycnal approached 70 m. As the tide reversed (survey section 3f), the feature began to move onto the bank. Its amplitude remained as large as 50 m, with a steep trailing edge. At maximum on-bank flow (survey section 3g), it had traveled over 10 km onto the bank through a combination of propagation and advection, and was substantially reduced in amplitude to 25 m, although its shape appeared to retain the steep trailing edge. Taking tidal advection into account, a propagation speed for this feature is estimated to be 0.17 m s^{-1}, close to the mode 1 phase speed (calculations described below). Survey sections 3e–3g are from different longitudes, so it could be argued that the observations used in calculating this phase speed are not necessarily of the same feature, or that its location has some east-west variation. It should be noted, however, that if the location of these observations are tidally advected to a common time (section 2.3; Figure 8), their effective east-west separation was at most 6 km.

[32] During on-bank flow, there was a tendency for dense water to dome upward over the slope, pinching off surface waters over the bank from those in the Gulf of Maine (lines 4a, 2a, 3g, 3d, 4b). The on-bank-propagating, nonlinear internal wave tended to sit at the leading edge of this domed region (lines 4a, 4b, 3g). A tongue of warm, saline MDW was pushed up onto the bank as the downward slanting isopycnals marking its upper boundary interacted with the slope (line 2a).

4.4. Comparisons Between On- and Off-Bank Flow

[33] Although the distortion of isopycnals near the bank edge showed similarities between on-bank and off-bank flow, the features generated during on-bank flow tended to be less steep than those generated during off-bank flow. Between the summit of Georges Bank and the Gulf of Maine, both bottom depth and stratification increase rapidly. Continuity of cross-bank flux requires that this component of tidal velocity is lower in the gulf, and stronger stratification leads to higher internal wave phase speeds. These factors combine to produce a pronounced contrast in Froude number (Figure 12) between the bank and the gulf, a pattern which is similar during on- and off-bank flow. In Figure 12, Froude numbers are calculated at 4-min intervals on the cruise path. Note that although Froude number is clearly strongly dependent on tidal phase, and all phases are included in Figure 12, the contrast between the shallow bank and deeper water to the north dominates even this. Cross-bank tidal flows are strongly supercritical to mode 1, $Fr_1 = O(10)$, over the bank and strongly subcritical to

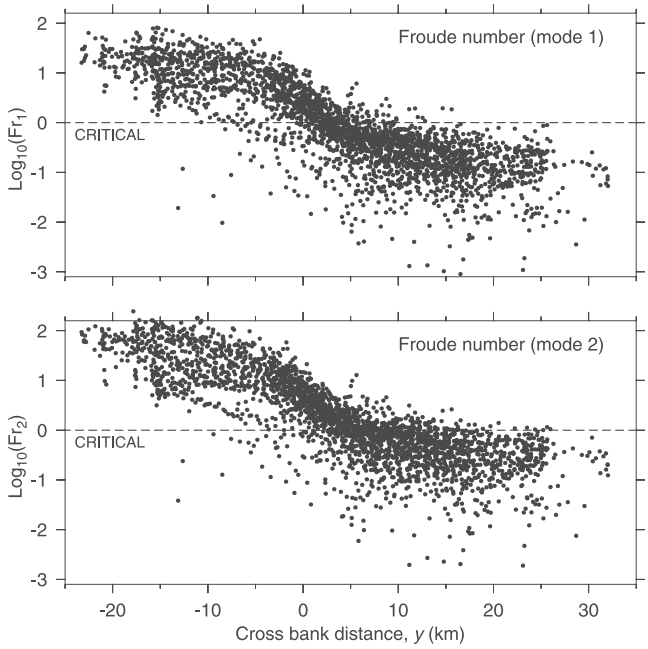

Figure 12. Froude numbers $\mathrm{Fr}_i = |\hat{v}/c_i|$ for the first two internal wave modes as a function of cross-bank position y. A log scale is used. Data points are at 4-min intervals, covering all SeaSoar observations. All phases of the tide are included (see Figure 4 for possible phase biases).

mode 1, $\mathrm{Fr}_1 = O(0.1)$ in the Gulf of Maine. Although Froude number is zero (so Log(Fr) = $-\infty$) at the instant when the Cross-bank component of the tide reverses, such low values evidently occur for a short time and do not figure significantly in Figure 12. The bank edge ($0 < y < 5$ km) is a transitional, near-critical zone for mode 1. Mode 2 phase speeds are lower, but again critical transition tends to occur in the slope region.

[34] Despite the fact that the pattern of criticality is similar during on- and off-bank flow, the direction of flow is important. In both cases, internal wave energy propagating against the mean flow can be stalled in the near-critical region. An important distinction, however, is that this energy tends to converge in the near-critical region when flow goes from supercritical to subcritical (off-bank flow) but diverge when flow goes from subcritical to supercritical (on-bank flow). Convergence occurs during off-bank flow because internal waves are able to propagate upstream against the subcritical flow in deep water, whereas waves propagating against the supercritical flow on the bank are swept downstream into the near-critical region.

[35] Cross-bank sections from times of near peak off- and on-bank flow are shown in detail in Figure 13. These are lines 2a and 3e of Figure 10, and both occurred at times when the outer bank was stratified. In both cases, flow over the bank was strongly supercritical to both modes 1 and 2. Mode 1 became critical near the bank edge and mode 2 farther off-bank. In the example during off-bank flow, mode 1 was near-critical in a 10-km region extending into deep water from the bank edge. Both sections show considerable distortion of the density field on the deep water side of the bank edge, resulting from interaction between the tidal advection and topography. The impression is that this internal structure is steeper during off-bank flow than during on-bank flow, with development of a feature resembling a hydraulic jump. The two sections are relatively typical in these respects (Figure 10). A hydraulic jump occurs at a transition from supercritical to subcritical flow, which here can only occur during off-bank flow. At a hydraulic jump, the existence of the subcritical downstream state cannot be communicated upstream (by wave propagation), so the adjustment (jump) is sudden, and may be turbulent.

[36] The bottom panels of Figure 13 show the depth-varying component of off-bank ADCP velocity $v_{bc} = v - \hat{v}$, where $\hat{v}$ is the depth mean over the vertical range of the ADCP data. The structure of v_{bc} reflects both internal wave perturbations, frictional modification of the tide near the bed, and nontidal velocity perturbations. It should not be regarded as a baroclinic velocity component decoupled from the barotropic flow, since such a decoupling is not valid in a region of sloping bottom topography, even in linear theory. The section during off-bank tidal flow (Figure 13a) shows a strong depth-varying velocity component, with an apparent mode 2 vertical structure (two zero crossings), in the region centered around 42.2°N, where wave-like perturbations of the density structure are also seen. The section during on-bank flow (Figure 13b) also shows apparent mode 2 vertical structure of the velocity field in a region of distorted isopycnals, in this case centered closer to the bank edge, at 42.16°N.

[37] Internal wave characteristics have been calculated for the M2 frequency (selected characteristics are shown as a mesh in Figure 13). These ray paths locally have a gradient $\alpha = \sqrt{(\sigma_{M2}^2 - f^2)/(N^2 - \sigma_{M2}^2)}$ and for a localized energy source, such as the bank edge, would trace co-phase lines in the direction of energy propagation. If the internal wave field were dominated by such propagation, sign reversals of v_{bc} would be expected to lie along characteristics, since these would be co-phase lines of the velocity structure. There is no clear ray structure in the two sections of Figure 13, and these sections are typical in this respect. In the section during off-bank flow, a band of positive off-bank v_{bc} traces a path from the bank edge onto the bank and apparently reflects from the surface. Although this feature has a substantially shallower gradient than the local internal wave characteristics, it may represent a ray path distorted by tidal advection relative to its source. Note that peak off-bank flow is strongly supercritical to internal wave propagation, so propagation onto the bank is not possible at such times.

4.5. Mean Sections in the Two-Dimensional Approximation

[38] Mean sections of temperature, salinity, density and the horizontal velocity components have been calculated by the phase-averaging method described in section 3.4. The mean density structure (Figure 14) shows stratification decreasing to the south (on-bank) with a slight (10 to 20 m) doming of isopycnals over the bank edge. Gradients within this mean are clearly less than is typical of the raw sections (Figures 9 and 10) due to the effect of averaging over tidal advection and other variability. The density structure is dominated by salinity. Temperature is coldest at the surface and increases with depth, although its vertical gradient is small in the upper 50 m of the water column.

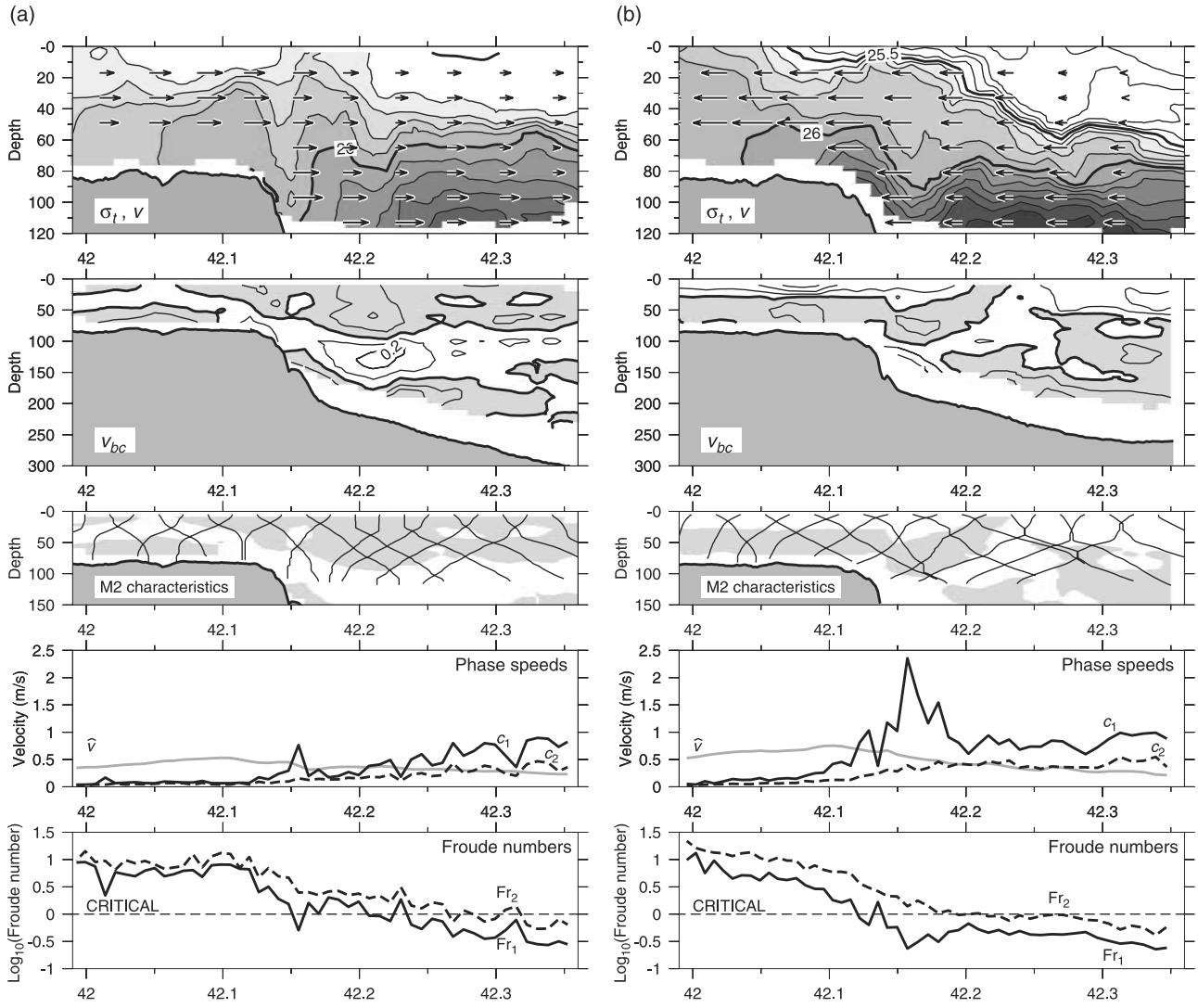

Figure 13. Density and velocity structure related to Froude number during (a) off-bank and (b) on-bank flow. Survey sections are 3e and 2a, respectively, of Figure 10. The top panels show density with vectors of the instantaneous ADCP v. The second row shows v_{bc}, in which the depth mean has been removed (shaded is on-bank, and contour interval is 0.1 m s^{-1}). In the third row, internal wave characteristic ray paths are shown for the M2 frequency, with background shading representing the sign of v_{bc}. In the fourth row, phase speeds of the lowest two vertical structure modes are calculated from equation (2) using the observed density profile, and compared with the instantaneous depth mean ADCP velocity $\hat{v}$ (shaded line) leading to a Froude number (fifth row).

[39] The mean (Eulerian) along-bank velocity component (u) shows an eastward jet with velocities exceeding 0.2 m s^{-1} at its core, 10–15 km north of the bank edge and at a depth of 60 m. This mean has a standard error of ±0.03–0.06 m s^{-1} for individual spatial bins ($\Delta z = 5$ m, $\Delta y = 1$ km; see section 3.4), although smoothing reduces the effective standard error to 0.01 m s^{-1} at most. The mean cross-bank (northward) velocity component (v) of up to 0.06 m s^{-1} has a similar effective standard error, so the weak on-bank (southward) flow on the bank and in the upper water column over the slope is significant.

[40] The subsurface maximum of along-bank velocity (u) coincides with the zero contour of the cross-bank density gradient $\partial\sigma_t/\partial y = 0$, suggesting that a thermal wind balance may be important. Geostrophic velocities (u_g) have been calculated based on the mean density field and referenced to ADCP velocities (u_{ref}) at 120 m or the deepest available (bold dashed line in Figure 14). A linear regression between the predicted thermal wind shear ($u_g - u_{ref}$) and shear of the observed mean velocity ($u - u_{ref}$) for the gridded fields of Figure 14 in the region $y \geq 5$ km (off-bank) has a gradient of close to unity (1.083), with the thermal wind balance predicting a slightly greater vertical shear than was observed. Subtracting the predicted geostrophic velocity field from the mean ADCP velocity in this region removes 92% of its variance. Over the bank and close to the bank edge ($y < 5$ km) there is no significant correlation between $u_g - u_{ref}$ and $u - u_{ref}$.

[41] The standard deviation of density (Figure 15) from the phase-averaged density field represents both temporal

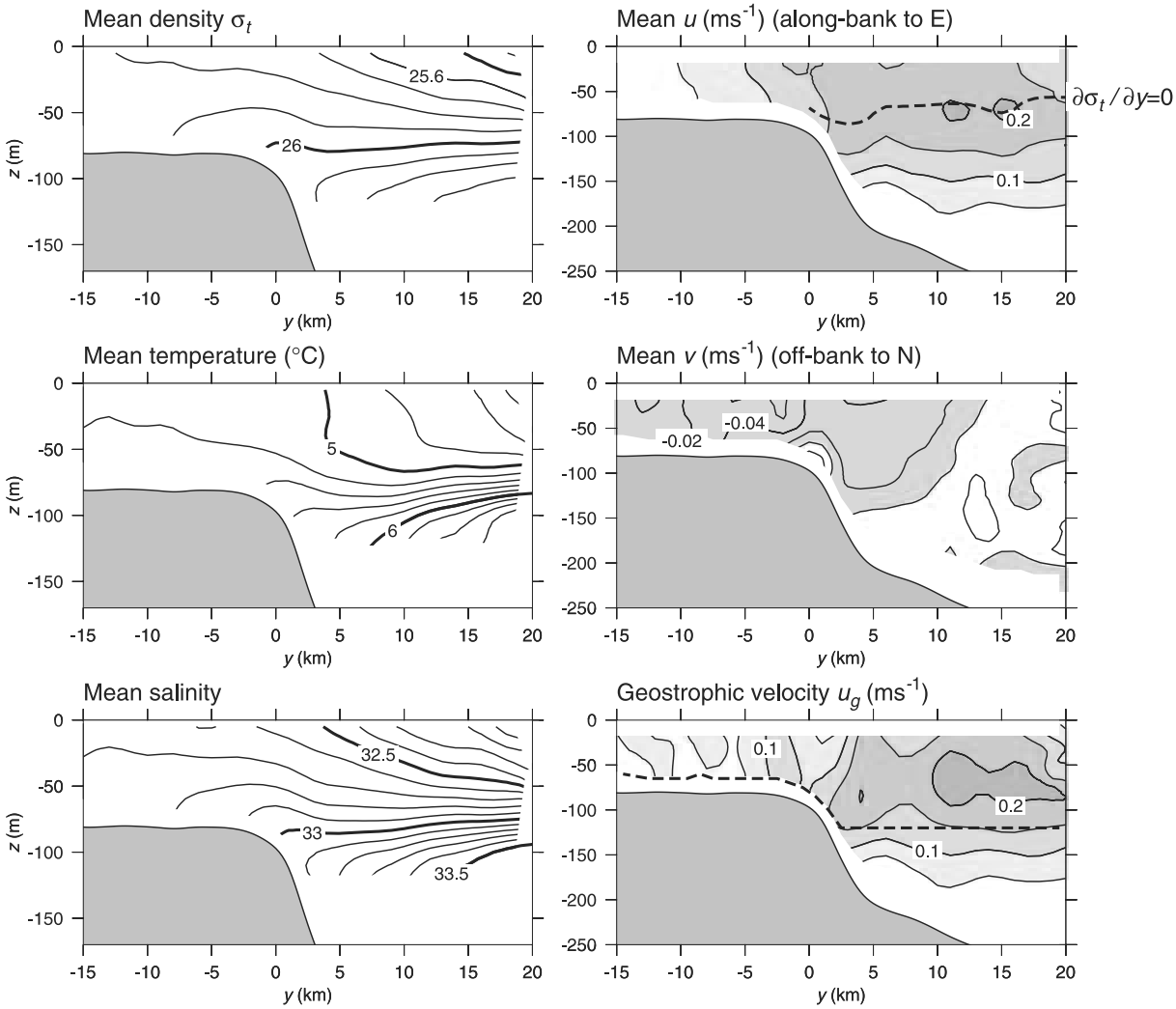

Figure 14. Phase-averaged mean sections of density (σ_t), temperature, salinity, Eulerian velocity components (u, v), and geostrophic along-bank velocity (u_g) in the standard coordinate system (y, z). Maximum standard errors are less than 0.01 kg m^{-3} (σ_t), and around 0.01 m s^{-1} (u, v). Geostrophic velocities are calculated using the mean σ_t referenced to ADCP velocities at 120 m or the deepest available (thick dashed line). Shading of v shows sign (shaded is on-bank), and of u and u_g shows amplitude.

and spatial (along-bank) variability. Tidal effects dominate, with high values both where dense water and strong gradients are advected back and forth across the bank edge, and in the pycnocline where internal wave perturbations are greatest. Surface-intensified variability over the bank and off-bank is due to the intermittent presence of SSW.

4.6. M2 and M4 Tide in the Two-Dimensional Approximation

[42] The M2 velocity component derived from harmonic analysis (section 3.5) represents much of the variance of the observed ADCP velocities. The proportion of the variance of v that is explained by M2 ranges from 90% over the bank to 20% near the surface in the Gulf of Maine ($y > 15$ km). These figures are consistent with a relatively even distribution of non-M2 variance, with M2 representing a greater proportion of the total variance in areas where its amplitude is large (on the bank).

[43] Cross-bank M2 velocity v_{M2} is maximum on the bank, reaching 0.7 m s^{-1} and largely barotropic (Figure 16), for a total tidal excursion of 10 km. Amplitude decreases and phase advances slightly toward the bed (Figure 17), but not to the extent seen by *Loder et al.* [1992] in similar analyses of shipboard and ADCP data from summer. Vertical structure of the cross-bank velocity field increases with distance off-bank. The phase lead of v_{M2} near the bottom peaks at around 40° over the lower slope, although the z-dependence of amplitude continues to increase offshore.

[44] Performing a similar M2 analysis of the "baroclinic" crossbank velocity (here taken to be the ADCP velocity with its instantaneous depth mean removed: $v_{bc} = v - \hat{v}$) reveals a mid-water-column phase reversal (Figure 16). The depth of this phase reversal reflects the shape of the topography, shoaling from around 110 m in deep water ($y > 10$ km), to 30 m over the bank. Amplitude of v_{bc} is small on the bank, and off-bank is small close to the mid-

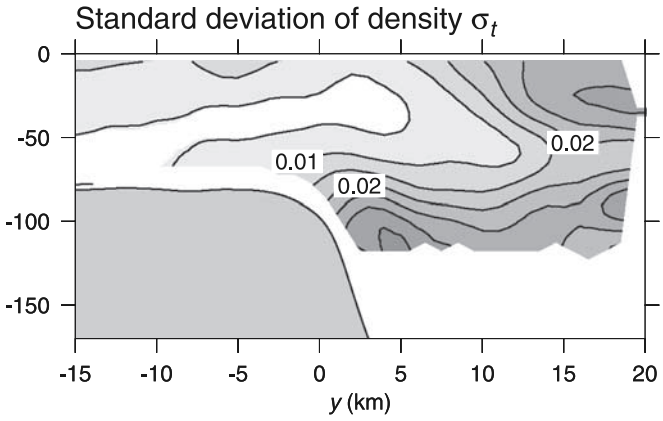

Figure 15. Phase-averaged standard deviation of density (σ_t) in the standard coordinate system (y, z).

water-column phase reversal. At y = 20 km, v_{bc} peaks at around 0.15 m s^{-1} near the surface and bed and, since these points are antiphase, there is an instantaneous velocity range of up to 0.3 m s^{-1}, of the same order as the depth mean tidal velocity. Near the surface, barotropic and baroclinic components of v_{M2} are of similar amplitude and antiphase, so the total v_{M2} is near-zero, although $u_{M2} \approx 0.25$. Solving the vertical eigenvalue problem (2) at the M2 frequency for stratification typical of $y > 15$ km gives a mode 1 (2) wavelength of 52 km (25 km) and phase speed of 1.16 m s^{-1} (0.55 m s^{-1}). The observed rate of phase increase with y in the upper water column is consistent with off-bank-propagation of a mode 1 internal wave at the M2 frequency. Over the slope ($0 < y < 10$ km), v_{bc} shows large values at the M2 frequency, but these correspond to a decrease in amplitude and phase lead of the total tidal velocity v_{M2}. It is not clear whether these features represents internal tidal dynamics or frictional effects.

[45] The M4 constituent (period 6.21 hours) is the first "overtone" of M2 and reflects the nonsinusoidal nature of the lunar tide. Although this may be indicative of regions of nonlinearity, the presence of an M4 velocity signal should be interpreted with caution. Advection of a propagating (linear) M2 internal wave by an M2 frequency background current would produce a distorted M2 velocity signal when observed from a fixed location, introducing an M4 component. In mooring data from the Northern Flank of Georges Bank, *Magnell et al.* [1980] have observed substantial energy at M2 harmonic frequencies. In our M4 analysis, amplitude of crossbank velocity v_{M4} (Figure 18) is highest over the bank (where $|M4|/|M2| \approx 0.1$) and close to the bottom in deeper water, particularly in the region of maximum bottom slope (again, $|M4|/|M2| \approx 0.1$). Elevated values also occur in deep water ($y > 15$ km) both in the pycnocline and near the surface.

5. Discussion and Summary

[46] During the survey period (spring 1999), considerable variability was observed as a result of the episodic presence of Scotian Shelf Water (SSW) at the surface. The reason for this variability was a large and evolving patch of SSW that lay immediately to the northeast of the survey region in the Northeast Channel (Figure 6). Cool, fresh water, presumably with a substantial influence from SSW, was observed at the surface north of the bank edge at all times during the surveys. Over Georges Bank, this water was intermittently present, and when it was present it was found predominantly in the east. The variability (both spatial and temporal) of SSW-induced stratification means that, even with 35 cross-bank sections, it is difficult to determine the features of a "typical" tidal cycle at this time of year. A natural partition of these observed sections has been made, between those in which the bank was stratified and those in which it was well-mixed, although within these two partitions there is still considerable variation. Figures 9 and 10 show lines ordered by tidal phase and should be viewed as a summary of the features observed at various tidal phases, with and without on-bank stratification, rather than as a representation of a particular tidal cycle.

[47] When SSW crosses the bank edge into shallow water, it apparently does so as a surface slab. During the surveys, the pycnocline associated with the base of this slab was at times near the surface (≈10 m, sections 2c, 3d, etc., of Figure 11) and at times as deep as the center of the water column (≈40 m, sections 3e, 3f, etc.). The density difference between the surface and bottom was 0.4 kg m^{-3} or less, around half that of typical thermally-induced summer stratification [e.g., *Loder et al.*, 1992]. The weaker stratification meant that internal wave propagation speeds on the outer bank during stratified periods of spring 1999 were slower than is typical in summer, and tidal flow on the bank tended even more strongly toward supercriticality. In other respects the thermally-stratified summer system and SSW-stratified spring system are very similar and a close analogy can be drawn here with summer observations [*Loder et al.*, 1992; *Brickman and Loder*, 1993] and modeling studies [*Lamb*, 1994; *Chen and Beardsley*, 1998].

[48] Internal tidal behavior on the Northern Flank of Georges Bank is characterized by advective velocities which, over the slope, are comparable to low-mode internal wave propagation speeds. The result is large amplitude internal features which develop primarily during off-bank flow. Georges Bank differs from other locations where strong, near-critical tidal flows have been described because it has a shelf-edge type topography, as opposed to an isolated bump or sill (such as in Knight Inlet [*Farmer and Smith*, 1980]). Behavior in these two cases is somewhat different. An isolated bump has a tendency to exert hydraulic control over subcritical upstream flow. This ensures that flow is critical over the summit and supercritical immediately downstream of it, where lee waves and hydraulic features develop. Similar features develop on the northern edge of Georges Bank, however in this case there is no possibility for hydraulic control of the supercritical upstream flow. Criticality occurs because the flow slows through continuity as it crosses the bank edge.

[49] At a summer tidal mixing front a balance develops between mixing processes and the buoyancy input from solar heating. *Brickman and Loder* [1993] have estimated that the rate of energy supply to the thermally stratified region of the Northern Flank of Georges Bank by tidally generated, on-bank-propagating, high-frequency internal waves is greater than that required to overcome solar heating and mix the water column vertically. Bottom stirring by tidal currents dominates both, although the efficiency with which this

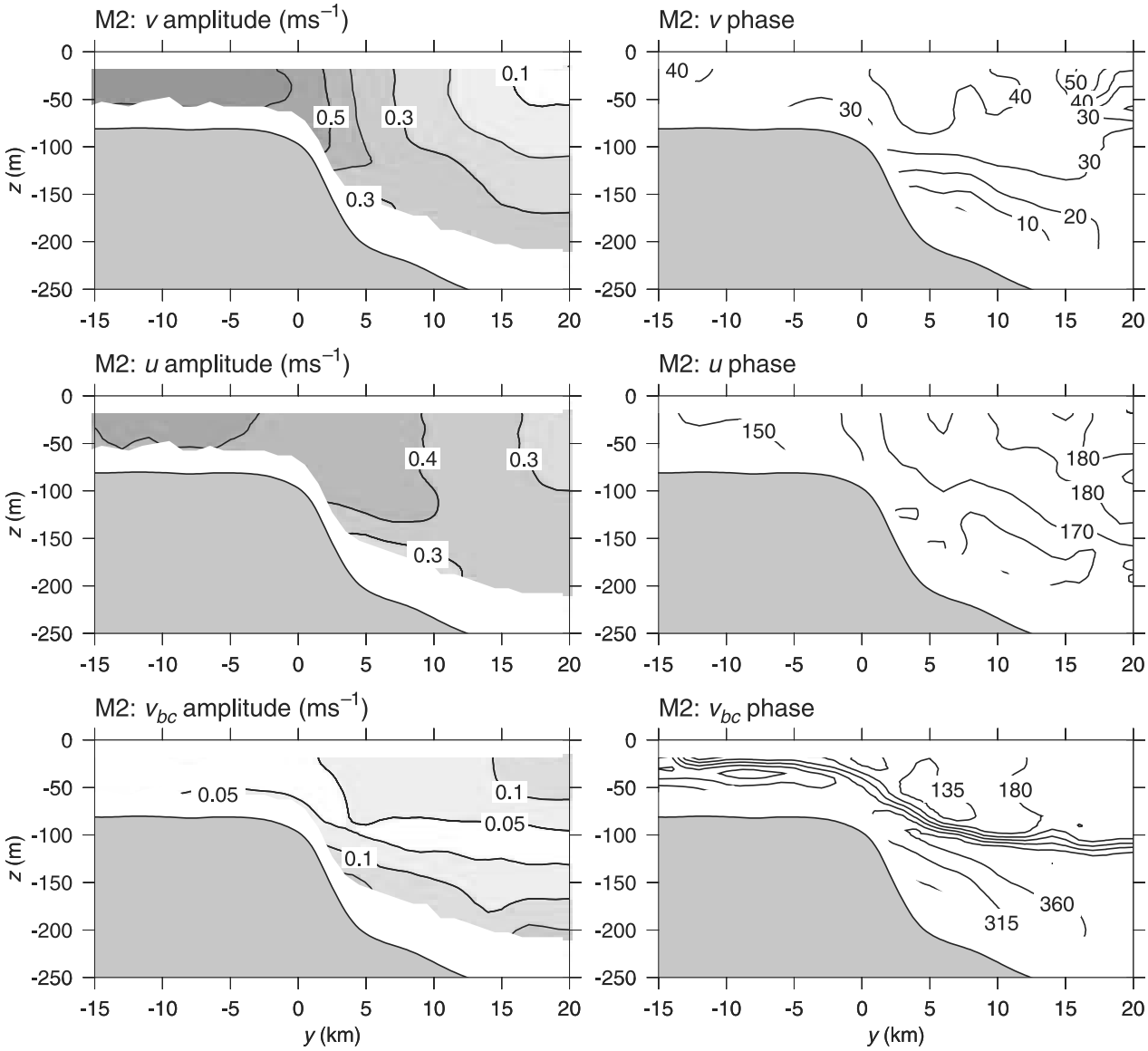

Figure 16. M2 amplitude and phase of u and v velocity components and of the "baroclinic" velocity $v_{bc} = v - \hat{v}$.

energy is converted to potential energy through mixing is low, permitting the deeper regions of the bank to remain stratified. The mixing efficiency of internal tidal energy when it encounters the tidal mixing front is unknown, although it is presumably greater than bottom stirring because it is concentrated in the pycnocline. It is also possible that not just nonlinear internal tidal features, but the linear internal tide too contributes to mixing at the front. In model simulations, *Chen et al.* [2003] found that a linear internal tide propagating toward a mixing front is refracted by the frontal density structure, becoming highly nonlinear and releasing energy to mixing, with little apparent reflection.

[50] During spring 1999, SSW provided an intermittent source of buoyancy to Georges Bank. A balance could not develop between this variable source and mixing processes, so the system was continually adjusting as buoyancy was supplied and progressively eroded by mixing processes acting to assimilate the SSW with ambient bank water. The modification of internal tidal behavior by stratification of the bank enabled a (possibly significant) mixing mechanism, the release of internal tidal energy at the on-bank limit of stratification. To relate the spring 1999 case to summer 1988, the energy required to vertically mix the stratified bank water of survey section 3h (one of the more strongly stratified sections encountered) (Figure 10) would be approximately 30 J m^{-3}. On the basis of the buoyancy supply estimates of *Brickman and Loder* [1993], an equivalent stratification would develop over 12 days of solar heating (with a surface heat flux of 165 W m^{-2}, typical of early summer).

[51] Horizontal resolution of the SeaSoar is not sufficient to provide a detailed picture of on- and off-bank-propagating high-frequency internal waves (or wave packets), although these features do appear as clear, localized disturbances. In July 1988 data, *Loder et al.* [1992] identified a pair of on-bank-propagating soliton-like depressions of the density structure on each tidal cycle, originating as a pair of lee-waves during off-bank flow. These features were repro-

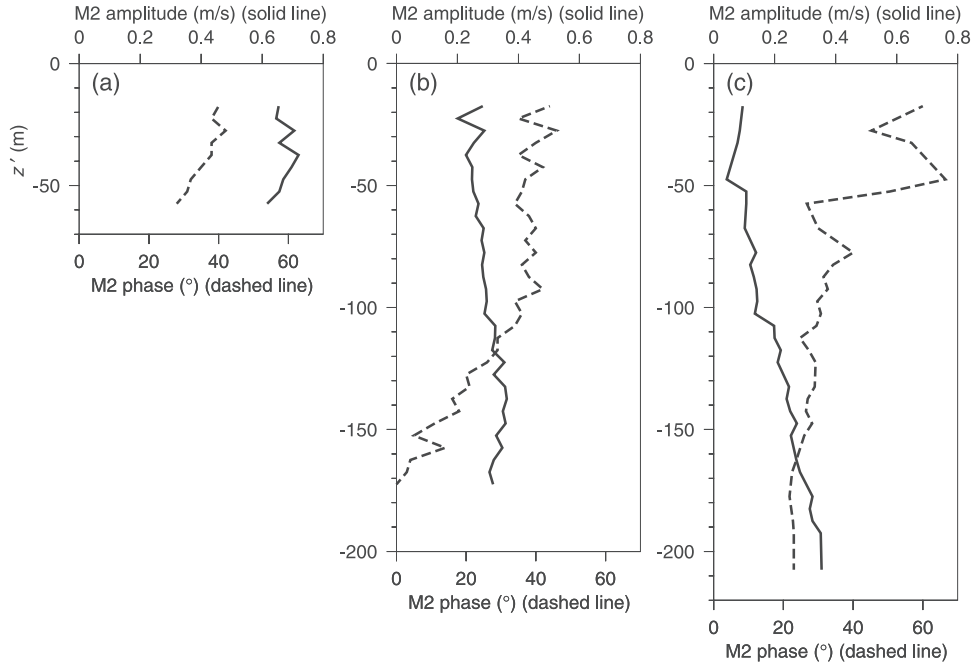

Figure 17. Vertical profiles of M2 amplitude and phase of v at (a) $y = -5$ km, (b) $y = 8$ km, and (c) $y = 17$ km.

duced in a modeling study by *Lamb* [1994]. At a mooring on the bank (10 km from the bank edge), the arrival time of the first of these depressions was predictable, but the second was more variable, and on some tidal cycles no such feature was observed [*Brickman and Loder*, 1993]. In the spring 1999 data set there is no evidence of such a pair of solitary waves. Survey section 3e (Figure 10) clearly shows a pair of lee waves during off-bank flow; However, the temporal sequence of survey sections 3e–3f–3g–3h subsequently shows only one on-bank-propagating feature. It is doubtful whether a second solitary wave could propagate sufficiently far on-bank, given the weaker spring stratification, to avoid being swept back into the slope region by supercritical off-bank flow.

[52] For the purpose of determining long-term mean and tidal structure, a collapse of the data set from three dimensions to two is justified by the fact that the topography (Figure 3), background hydrography, and tidal forcing are remarkably two-dimensional in this region. The (dominant) barotropic M2 tide propagates to the west along the northern edge of Georges Bank, so there is some east-west variation of phase. An estimate of this propagation speed, based on two pressure recorders separated by 130 km [*Brown and Moody*, 1987, their stations 2 and 6], implies a 17° phase difference between eastern and western edges of our survey grid (40 km). The barotropic tidal analysis described in section 3.2, using data more specific to the actual survey region, suggests a slower westward phase propagation, in this case of on-bank velocity (v), with a phase difference of around 10° across the survey grid, and little change in the cross-bank flux. These estimates support the assertion that tidal forcing is relatively uniform along the bank edge on the scales of interest here. As far as the uniformity of hydrographic fields is concerned, analysis of near-surface fields (Figures 8 and 11) is considered a severe test, since presumably topographic constraints are weakest near the surface, wind effects are significant, and patchy SSW is present. Nevertheless, mean fields of temperature at 5 m and depth of the 32.5 psu isohaline (Figure 11) show a clear dominance of $\partial/\partial y$ over $\partial/\partial x$ by a factor of around 5. This does not hold over the bank. Further support for the two-dimensional simplification comes from the mean velocity fields (Figure 14), where the along-bank component strongly dominates the cross-bank component by an order of magnitude to the north of the bank edge. On the bank, the two velocity components are of similar magnitude, again suggesting that the bank dynamics are not well represented by two dimensions.

[53] Having supplied justification for collapsing this data set to two dimensions, some caution should clearly be exercised in the interpretation of mean fields of a complex and variable system. Several robust results do, however, emerge from the two-dimensional analysis: a mean along-bank flow of a little over 0.2 m s^{-1}, which appears to be in thermal wind balance with the mean density structure, and some broad aspects of the M2 internal tidal structure. Finescale and variable features of the internal tidal structure are not represented.

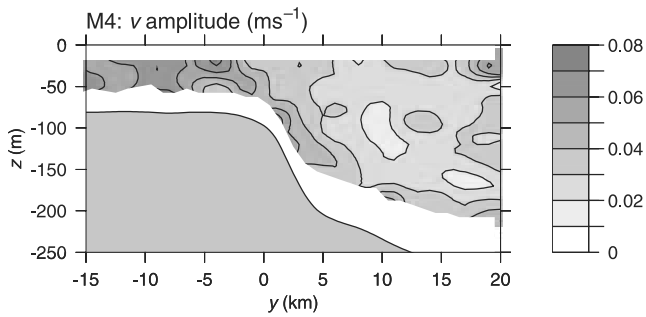

Figure 18. M4 amplitude of cross-bank velocity v.

[54] The harmonic analysis of velocities at the M2 frequency (Figure 16) is of most significance north of the bank edge, where stratification is less variable than on the bank and presumably the phase structure of the internal tide is more predictable. There is clear evidence, in the mid-water-column phase reversal of ''baroclinic'' velocity and in the off-bank phase propagation, of a mode 1 internal wave that travels to the north into the Gulf of Maine. There is also evidence of modification of tidal velocities over the slope, where total tidal velocities are lower than higher in the water column and lead them in phase. These ''baroclinic'' tidal velocity fields should be interpreted with caution, however, as they represent vertical structure which can result from frictional effects in addition to internal wave dynamics.

[55] Instantaneous crossbank ''baroclinic'' velocities (Figure 13) show much structure that is not evident in the harmonic analysis. Indeed, it is often difficult to discern the mode 1 structure that emerged so clearly from that analysis, although propagation in a ray-like manner along internal wave characteristics is not clear either. There is evidence of the stalling of high-frequency internal waves over the slope during both on- and off-bank flow. These stalled waves are of higher than mode 1 structure, with at least two sign changes in the vertical. While these features are related to the M2 tide, they do not appear in the harmonic analysis partly because of the discarding of non-M2 frequencies, and partly because of smoothing arising from the variability of the system and perhaps the vertical distortion inherent in collapsing the three-dimensional data set to two dimensions. In particular, and not surprisingly, the harmonic analysis does not reveal internal tidal structure on the bank where variability is greatest and the two-dimensional analysis least justifiable.

[56] The picture that emerges from this data set is that the frontal system on the Northern Flank of Georges Bank is controlled by mixing due to the intense and highly nonlinear tide. In spring, considerable variability is introduced by the episodic presence of SSW which stratifies the bank. Changes in stratification lead to modification of the internal tide, enabling mixing processes which work to assimilate the SSW with Georges Bank Water. There appears to be considerable potential for water (and biota) from the Gulf of Maine to travel onto the bank, both at the surface, as described above, and deeper through the complex tidal dynamics and mixing that occur near the steeply sloping edge of the bank. Mixing and cross-frontal fluxes are considered in greater detail in part two [*Ullman et al.*, 2003].

[57] **Acknowledgments.** We thank Marc Willis and Linda Fayler, OSU Marine Technicians, who were responsible for the success of the SeaSoar operations. We also thank the officers and crew of R/V *Oceanus* for their help in making continuous SeaSoar operations possible. Post-processing of the SeaSoar data was performed by Bob O'Malley (OSU). Sandy Fontana (URI) carried out the processing of the ADCP data. The SST images (Figure 6) were supplied by J. J. Bisagni (U. Mass., Dartmouth). This work was supported by NSF grants OCE9806650 and OCE9813641 and is contribution 378 of the U.S. GLOBEC program.

References

Barth, J. A., S. D. Pierce, and R. L. Smith, A separating coastal upwelling jet at Cape Blanco, Oregon and its connection to the California Current system, *Deep Sea Res., Part II*, *47*, 783–810, 2000.

Bisagni, J. J., and P. C. Smith, Eddy-induced flow of Scotian Shelf Water across Northeast Channel, Gulf of Maine, *Cont. Shelf Res.*, *18*, 515–539, 1998.

Bisagni, J. J., R. C. Beardsley, C. H. Ruhsam, J. P. Manning, and W. J. Williams, Historical and recent evidence of Scotian Shelf Water on southern Georges Bank, *Deep Sea Res., Part II*, *43*, 1439–1471, 1996.

Brickman, D., and J. W. Loder, Energetics of the internal tide on northern Georges Bank, *J. Phys. Oceanogr.*, *23*, 409–424, 1993.

Brown, W. S., and J. A. Moody, Tides, in *Georges Bank*, edited by R. H. Backus, pp. 100–107, MIT Press, Cambridge, Mass., 1987.

Butman, B., R. C. Beardsley, B. Magnel, D. Frye, J. A. Vermersch, R. Schlitz, R. Limeburner, W. R. Wright, and M. A. Nobel, Recent observations of the mean circulation on Georges Bank, *J. Phys. Oceanogr.*, *12*, 569–591, 1982.

Butman, B., J. W. Loder, and R. C. Beardsley, The seasonal mean circulation: Observation and theory, in *Georges Bank*, edited by R. H. Backus, pp. 125–138, MIT Press, Cambridge, Mass., 1987.

Candela, J., R. C. Beardsley, and R. Limeburner, Separation of tidal and subtidal currents in ship-mounted acoustic Doppler current profiler observations, *J. Geophys. Res.*, *97*, 769–788, 1992.

Chen, C., and R. C. Beardsley, Tidal mixing and cross-frontal particle exchange over a finite amplitude asymmetric bank: A model study with applications to Georges Bank, *J. Mar. Res.*, *56*, 1163–1201, 1998.

Chen, D., H. W. Ou, and C. Dong, A model study of internal tides in coastal frontal zone, *J. Phys. Oceanogr.*, *33*, 170–187, 2003.

Farmer, D. M., and J. D. Smith, Tidal interaction of a stratified fluid with a sill in Knight Inlet, *Deep Sea Res., Part A*, *27*, 239–254, 1980.

Flagg, C. N., Hydrographic structure and variability, in *Georges Bank*, edited by R. H. Backus and D. W. Bourne, pp. 108–124, MIT Press, Cambridge, Mass., 1987.

Hannah, C. G., C. E. Naimie, J. W. Loder, and F. E. Werner, Upper-ocean transport mechanisms from the Gulf of Maine to Georges Bank, with implications for Calanus supply, *Cont. Shelf Res.*, *17*, 1887–1911, 1997.

Houghton, R. W., and R. G. Fairbanks, Water sources for Georges Bank, *Deep Sea Res., Part II*, *48*, 95–114, 2001.

Lamb, K. G., Numerical experiments of internal wave generation by strong tidal flow across a finite amplitude bank edge, *J. Geophys. Res.*, *99*, 843–864, 1994.

La Violette, P. E., D. R. Johnson, and D. A. Brooks, Sun-glitter photographs of Georges Bank and the Gulf of Maine from the space shuttle, *Oceanography*, *3*, 43–49, 1990.

Loder, J. W., Topographic rectification of tidal currents on the sides of Georges Bank, *J. Phys. Oceanogr.*, *10*, 1399–1416, 1980.

Loder, J. W., and D. G. Wright, Tidal rectification and frontal circulation on the sides of Georges Bank, *J. Mar. Res.*, *43*, 581–604, 1985.

Loder, J. W., D. Brickman, and E. P. W. Horne, Detailed structure of currents and hydrography on the northern side of Georges Bank, *J. Geophys. Res.*, *97*, 14,331–14,351, 1992.

Loder, J. W., K. F. Drinkwater, N. S. Oakey, and E. P. W. Horne, Circulation, hydrographic structure and mixing at tidal fronts: The view from Georges Bank, *Philos. Trans. R. Soc. London, Ser. A.*, *343*, 447–460, 1993.

Magnell, B. A., S. L. Spiegel, R. I. Scarlet, and J. B. Andrews, The relationship of tidal and low-frequency currents on the north slope of Georges Bank, *J. Phys. Oceanogr.*, *10*, 1200–1212, 1980.

Marsden, R. F., The internal tide on Georges Bank, *J. Mar. Res.*, *44*, 35–50, 1986.

Mavor, T. P., and J. J. Bisagni, Seasonal variability of sea-surface temperature fronts on Georges Bank, *Deep Sea Res., Part II*, *48*, 215–243, 2001.

Naimie, C. E., Georges Bank residual circulation during weak and strong stratification periods: Prognostic numerical model results, *J. Geophys. Res.*, *101*, 6469–6486, 1996.

Simpson, J. H., and J. R. Hunter, Fronts in the Irish Sea, *Nature*, *250*, 404–406, 1974.

Ullman, D. S., A. C. Dale, D. Hebert, and J. A. Barth, The front on the Northern Flank of Georges Bank in spring: 2. Cross-frontal fluxes and mixing, *J. Geophys. Res.*, *108*(C11), 8010, doi:10.1029/2002JC001328, in press, 2003.

J. A. Barth and A. C. Dale, College of Oceanic and Atmospheric Sciences, Oregon State University, 104 Ocean Administration Building, Corvallis, OR 97331-5503, USA. (barth@coas.oregonstate.edu; acd@coas.oregonstate.edu)

D. Hebert and D. S. Ullman, Graduate School of Oceanography, University of Rhode Island, 215 South Ferry Road, Narragansett, RI 02882, USA. (dhebert@gso.uri.edu; d.ullman@gso.uri.edu)